J. Space Weather Space Clim. 2 (2012) A02
DOI: 10.1051/swsc/2012003

SWSC

Near-earth solar wind flows and related geomagnetic activity during more than four solar cycles (1963–2011)

Ian G. Richardson[1,2,*], and Hilary V. Cane[3]

[1] Code 661, NASA/Goddard Space Flight Center, Greenbelt, Maryland 20771, USA
*corresponding author: e-mail: ian.g.richardson@nasa.gov
[2] CRESST and Department of Astronomy, University of Maryland, College Park, Maryland 20742, USA
[3] School of Mathematics and Physics, University of Tasmania, Hobart, Tasmania, Australia

Received 27 February 2012 / Accepted 29 April 2012

ABSTRACT

In past studies, we classified the near-Earth solar wind into three basic flow types based on inspection of solar wind plasma and magnetic field parameters in the OMNI database and additional data (e.g., geomagnetic indices, energetic particle, and cosmic ray observations). These flow types are: (1) High-speed streams associated with coronal holes at the Sun, (2) Slow, interstream solar wind, and (3) Transient flows originating with coronal mass ejections at the Sun, including interplanetary coronal mass ejections and the associated upstream shocks and post-shock regions. The solar wind classification in these previous studies commenced with observations in 1972. In the present study, as well as updating this classification to the end of 2011, we have extended the classification back to 1963, the beginning of near-Earth solar wind observations, thereby encompassing the complete solar cycles 20 to 23 and the ascending phase of cycle 24. We discuss the cycle-to-cycle variations in near-Earth solar wind structures and the related geomagnetic activity over more than four solar cycles, updating some of the results of our earlier studies.

Key words. Stream – Solar cycle – Interplanetary Coronal Mass Ejection (CME) – Interplanetary medium

1. Introduction

In past studies (Richardson et al. 2000, 2001, 2002; Richardson 2006), we divided the near-Earth solar wind since 1972 into three basic flow types in order to assess, for example, the contribution of each type of solar wind flow to long-term (> ~solar rotation) averages of geomagnetic indices and the interplanetary magnetic field, and to determine the structures driving geomagnetic storms. The three flow types are:

- Corotating high-speed streams, typically with solar wind speed $V > \sim 450$ km s^{-1}, that originate in coronal holes at the Sun (Krieger et al. 1973; Zirker 1977). The properties of corotating high-speed streams near 1 AU were summarized by Belcher & Davis (1971) and include the formation of a region of compressed plasma, the "corotating interaction region" (CIR), at the leading edge of the stream as it interacts with the preceding slower, cooler, and denser solar wind. Since the source coronal holes may persist for longer than a solar rotation, a given stream may recur at the solar rotation period (~27 days as viewed from Earth).
- Slower, interstream solar wind, typically associated with the streamer belt at the Sun (e.g., Feldman et al. 1981); and
- Transient flows originating with coronal mass ejections (CMEs) at the Sun, including interplanetary coronal mass ejections (ICMEs), the manifestations in the solar wind of CMEs, and the associated upstream shocks and post-shock/sheath regions (see Zurbuchen & Richardson 2006 and references therein for discussion of the in-situ signatures of ICMEs). We collectively term these "CME-associated" flows.

In recent years, solar wind composition/charge state observations have been used to make a similar classification of flows during solar cycle 23 (Zhao et al. 2009). Unfortunately, such observations are not generally available for earlier cycles, so other data have to be used. In our studies, the solar wind flow classification is based on inspection of a variety of data. These include 1-hour averages of near-Earth solar wind parameters obtained from the OMNI2 (formally OMNI) database (http://omniweb.gsfc.nasa.gov/; King & Papitashvili 2005). The OMNI2 data extend back to 27 November 1963 and are compiled from observations made by various near-Earth spacecraft that have been carefully intercalibrated. OMNI2 data coverage is variable, with significant gaps in the early data, as will be discussed further below, and from 1983 until late 1994, when solar wind observations were predominantly made by IMP 8, which only spent part of each orbit of the Earth outside the Earth's bow shock. The ICME identifications made in our previous studies (e.g., Richardson & Cane 1993; Richardson & Cane 1995; Richardson et al. 1997; Cane & Richardson 2003; Richardson & Cane 2010) have been incorporated into the solar wind classification. However, because the data required to separate ICMEs from their upstream "sheaths" are not consistently available, in particular in near-Earth observations prior to solar cycle 23, we do not differentiate between these structures when classifying solar wind flows, referring to them collectively as "CME-associated" flows as noted above.

Geomagnetic activity data are also examined since activity may be enhanced during the passage of ICMEs and associated flows (e.g., Burlaga et al. 1981; Wilson 1987, 1998; Tsurutani et al. 1988; Gosling et al. 1991; Tsurutani & Gonzalez 1997;

Richardson et al. 2001; Zhang et al. 2007; Echer et al. 2008; Richardson & Cane 2010, 2011a, and references therein), and also during the passage of high-speed streams past the Earth (e.g., Sheeley et al. 1976, 1977; Richardson 2006; Richardson et al. 2006; Tsurutani et al. 2006, and references therein). Examples will be illustrated below. Increased geomagnetic activity is associated with enhancements in the y-component of the solar wind convective electric field $E = -V \times B$, i.e., $E_y \sim VB_s$, where B_s is the southward magnetic field component, which leads to enhanced reconnection between solar wind and magnetospheric magnetic fields and enhanced energy deposition into the magnetosphere (e.g., Dungey 1961; Tsurutani & Gonzalez 1997; O'Brien & McPherron 2000; Ji et al. 2010, and references therein). In the case of CME-associated flows, the southward magnetic fields may be in the ICME and/or the upstream sheath formed between the ICME and associated shock (e.g., Tsurutani et al. 1988; Huttunen & Koskinen 2004; Zhang et al. 2007). In high-speed streams, intermittent intervals of southward fields associated with Alfvénic fluctuations moving out from the Sun result in geomagnetic activity that may persist for several days during passage of a stream past the Earth, and recur at the solar rotation period (e.g., Sheeley et al. 1976, 1977; Burlaga & Lepping 1977; Tsurutani & Gonzalez 1987; Tsurutani et al. 2006). Such activity can help to indicate the presence of streams when no solar wind speed observations are available. In addition, geomagnetic storm sudden commencements (SSCs) can help to identify the passage of interplanetary shocks at the Earth (Gold 1955), which may be generated ahead of fast ICMEs or CIRs, with the caveat that not all SSCs are caused by shocks (e.g., Gosling et al. 1967; Chao & Lepping 1974; Wang et al. 2006).

Energetic (~0.1–100 MeV) particle observations (principally made by Goddard Space Flight Center instruments on various near-Earth spacecraft) are also considered since these can help to indicate the passage of shocks and ICMEs. Solar particle event intensity time profiles often peak around shock passage, especially at lower energies, and then may fall abruptly as the ICME arrives a few hours after shock passage (e.g., Sanderson et al. 1990; Cane & Lario 2006; Klecker et al. 2006, and references therein). Modulations in the galactic cosmic ray intensity (i.e., "Forbush decreases"; Forbush 1937) can help to identify the passage of shocks and ICMEs (e.g., Barnden 1973a, 1973b; Cane et al. 1993, 1996; Cane 2000; Richardson & Cane 2011b, and references therein) and also corotating streams (Simpson et al. 1955; Iucci et al. 1979; Richardson et al. 1996; Simpson 1998; Richardson 2004, and references therein). We have used cosmic ray observations from neutron monitors and also from spacecraft, in particular the counting rate of the anti-coincidence guard of the Goddard instrument on IMP 8 (e.g., Cane 1993; Richardson et al. 1999). In summary, by combining these various data sets, we have been able to make a reasonably complete classification of the solar wind structures at Earth even when the solar wind data are not always complete.

Since these earlier studies, we have continued to update the solar wind flow classification to near-present. This has proved to be particularly valuable for studies of the magnetospheric and ionospheric response to different types of solar wind structures (e.g., Emery et al. 2009, 2011; Turner et al. 2009) and is available at the CEDAR workshop web site (http://cedarweb.hao.ucar.edu/wiki/index.php/Tools_and_Models:Solar_Wind_Structures). We have also recently extended the solar wind classification from 1972 back to 1963. This will be discussed in the next section, and examples of observations from this period will be illustrated. We then discuss the solar cycle variation in solar wind parameters and structures from 1963 to 2011. Section 4 summarizes the results of the paper.

2. Extension of the solar wind classification back to 1963/solar cycle 20

As noted above, solar wind observations incorporated into the OMNI2 database are available back to 1963 but our previous studies did not consider the period before 1972, when the observations become more complete (at least until 1983). Since these earlier observations encompass sunspot cycle 20, the weakest cycle so far during the space era, and with cycle 24 also expected to be a relatively weak cycle (e.g., http://www.swpc.noaa.gov/SolarCycle/SC24/index.html), we have extended the solar wind flow classification back from 1972 to the beginning of in-situ observations. Figure 1 shows the OMNI2 data coverage each year during 1963–1973 for various solar wind parameters together with the sunspot number, showing solar cycle 20. Data coverage varied greatly during this period and with solar wind parameter. While improving with time until 1967–1968, when coverage was comparable to post-1972 levels, there was a decline in 1969–1971, in particular in the availability of plasma density and temperature observations. Sunspot maximum in cycle 20 occurred in March 1969. Thus, more comprehensive solar wind observations are available in the ~2 years before solar maximum than in the similar period following maximum.

As discussed above, to help infer the structures present when limited or no solar wind observations are available, we used geomagnetic data (e.g., the *aa*, Mayaud 1972; *Kp*, Menvielle & Berthelier 1991; and *Dst*, Sugiura 1964, indices), energetic particle data (in particular from Goddard instruments on various spacecraft, e.g., Van Hollebeke et al. 1974 show observations

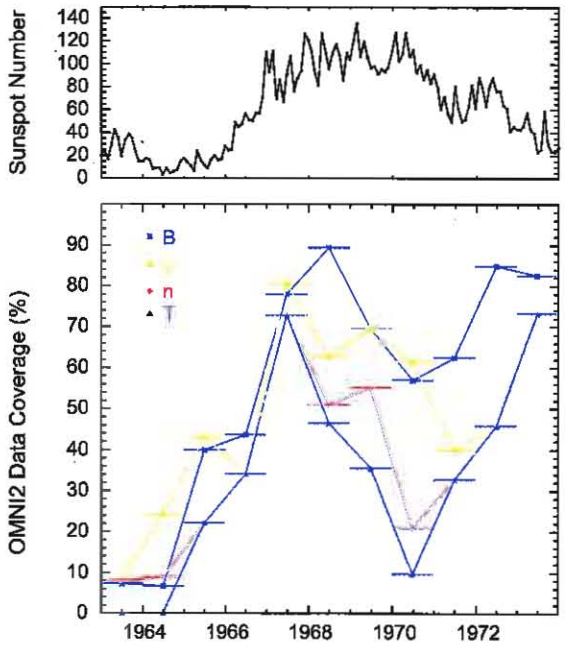

Fig. 1. OMNI2 data coverage in 1963–1973 for the interplanetary magnetic field intensity (B), solar wind speed (V), density (n), and proton temperature (T). The top panel shows the sunspot number, including solar cycle 20.

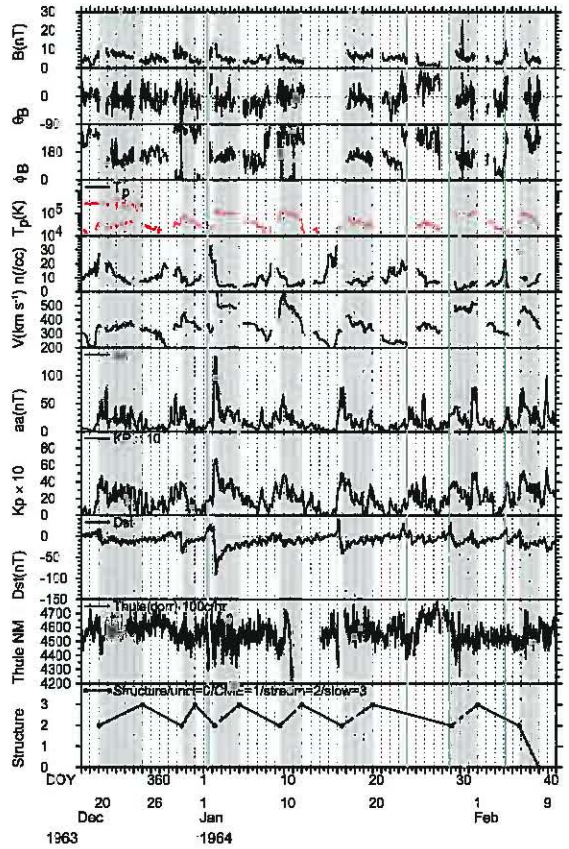

Fig. 2. OMNI2 solar wind parameters, geomagnetic indices, and neutron monitor data for a two solar rotation period in December 1963–February 1964. The panels show: the magnetic field intensity and polar and azimuthal angles (GSE coordinates), solar wind proton temperature (not available for this period), and expected temperature (red graph; see Richardson & Cane 1995 for further details), density, and speed, the geomagnetic *aa*, *Kp* × 10, and *Dst* indices, the Thule neutron monitor counting rate (pressure-corrected) and our assessment of the solar wind structure type, indicated at the *beginning* of the structure interval, where 2 is a high-speed stream, 3 is slow solar wind, and 0 indicates that the structure type is unclear. Gray shading indicates a series of corotating high-speed streams. Vertical green lines indicate times of SSCs, typically associated during this interval with CIRs.

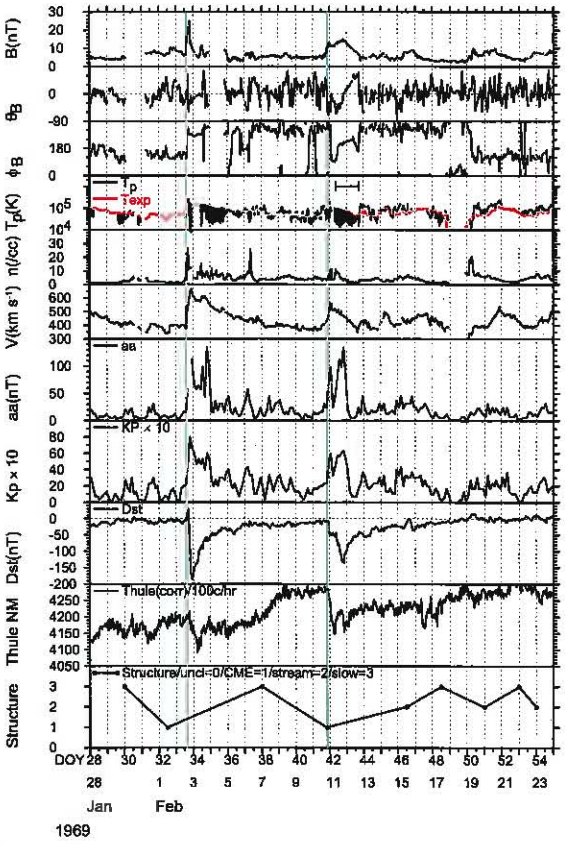

Fig. 3. Observations in a similar format to Figure 2 for a solar rotation period in January–February 1969 (sunspot number = 121). In the bottom panel, 1 = the start of a CME-associated interval.

in 1967–1972 from IMPs 4 and 5) and neutron monitor data. Figure 2 shows an example of OMNI2 solar wind magnetic field and plasma observations (from IMP 1) during a 54-day (~2 solar rotation) interval in November 1963–February 1964, close to the beginning of near-Earth solar wind monitoring. Geomagnetic indices (*aa*, *Kp* × 10, *Dst*) and neutron monitor data (from the Thule neutron monitor, http://neutronm.bartol.udel.edu/) are also shown. The bottom panel indicates our assessment of the start times of each type of solar wind flow, where 0 = unclear, 1 = CME-associated, 2 = corotating high-speed stream, and 3 = slow solar wind. During this period, observations were fairly complete though no proton temperature (T_p) data are available. Gray shaded regions indicate probable corotating streams that, in this case, formed a four stream/four magnetic sector/rotation configuration. (Note that the magnetic field reverses in each successive stream, where $\varphi_B \sim 135°$ indicates outward spiral magnetic fields, and $\varphi_B \sim 135°$, Sunward spiral fields, in GSE coordinates.) Corotating interaction regions, indicated by enhancements in the magnetic field strength and density, encompass the stream leading edges. Unshaded regions are predominantly slow solar wind. No CME-associated flows appear to have been present in this interval, near solar minimum (sunspot number for January 1964 was 15.3). Note that solar wind speeds in several of the indicated streams are unusually low compared to the usual criterion for a "high-speed" stream. For example, the observations suggest that the first stream indicated in Figure 2 apparently barely attained 400 km s^{-1}. Nevertheless, the pattern of slower and faster solar wind flows can still be discerned.

Figure 2 also illustrates how geomagnetic activity tends to be enhanced during the passage of high-speed streams, with the highest levels occurring in the vicinity of the CIRs, as is typical (e.g., Tsurutani et al. 2006). As noted above, such observations can help to indicate the presence of high-speed streams when limited solar wind observations are available. Similarly, the cosmic ray intensity may decrease during passage of a stream (Richardson 2004 and references therein) and provide another indication of the presence of a stream, though such decreases are not particularly clear in the fluctuating Thule data in Figure 2.

Figure 3 shows OMNI2, geomagnetic and cosmic ray observations during a solar rotation interval in January–February 1969 (sunspot number = 121), near solar maximum, in a similar format to Figure 2. The bottom panels again show the estimated start times of each type of solar wind structure where 1 = CME-associated flows; 2 = corotating high-speed streams; and

3 = slow solar wind. During this more active interval, ICMEs and associated flows are more prominent than during the interval in Figure 2. The two vertical green lines indicate SSCs that are associated with the passage of shocks. Following both shocks, proton temperature (T_p) depressions relative to the "expected" value for T_p (T_{exp}, red graph) based on the observed solar wind speed are observed. Black shading indicates where $T_p < 0.5T_{exp}$, which is often indicative of an ICME. (See rc95 for further discussion of T_{exp}, and its use in ICME identification.) The CME-associated flows are also associated with enhanced geomagnetic activity, and cosmic ray Forbush decreases. Note that the ICME on 11–12 February 1969 is the prototypical "magnetic cloud", an ICME with an enhanced magnetic field that rotates smoothly in direction suggestive of a flux-rope like magnetic field, identified by Klein & Burlaga (1982).

3. Solar cycle variations in near-earth solar wind structures and parameters during 1963–2011

Having extended the solar wind classification from near present back to 1963, we now investigate how the solar wind structures and parameters near the Earth have varied over more than four solar cycles. Figure 4 shows the monthly sunspot number together with three-solar rotation averages during 1963–2011 of the percentage of the time that the Earth was immersed in each type of solar wind flow, or whether the flow type was "unclear" (bottom panel). Note that we have been able to assess the structures that were present for much of cycle 20 using the combined data sets despite the incomplete OMNI2 data coverage. (The larger occurrence of unclear periods from 1983 to 1994 reflects the intermittent solar wind coverage from IMP 8.) The results indicate that the percentage of the time when the CME-associated flows are present tends to follow the solar activity/sunspot cycle, as would be expected given that the CME rate at the Sun follows the activity cycle (Webb & Howard 1994; Yashiro et al. 2004; Robbrecht et al. 2009). CME-associated flows occupied up to ~40–60% of the solar wind around solar maximum and were nearly absent (~5%) during solar minimum. Interestingly, the occurrence of CME-associated flows near the Earth does not appear to have been lower in the weaker sunspot cycles 20 and 23 compared to the larger cycle 21. (Cycle 22 is compromised by significant "unclear" intervals although the occurrence of CME-associated flows is similar to the other cycles.) Corotating high-speed streams are most prevalent during the decline of the cycle where they may form ~60% or more of the near-Earth solar wind. They are however present at all stages of the cycle. Slow solar wind is also present throughout the solar cycle and appears to have been most prevalent (~70%) during the most recent solar minimum, associated with a corresponding fall in the presence of high-speed streams. (See Russell et al. 2010 for a discussion of some of the notable features of this solar minimum.)

Figure 5 shows the variation in three-rotation averages of the *aa* index in all-solar-wind and in CME-associated flows, corotating streams, and slow solar wind, in 1963–2011. (Note the change of vertical scale in the bottom three panels.) We show *aa* (as in Richardson et al. 2000, 2002) since it is the index with the longest time series (since 1868) and is often used for long-term studies of geomagnetic activity and its relationship to other phenomena (e.g., Love 2011 and references therein). Although *aa* tends to be enhanced at times of higher

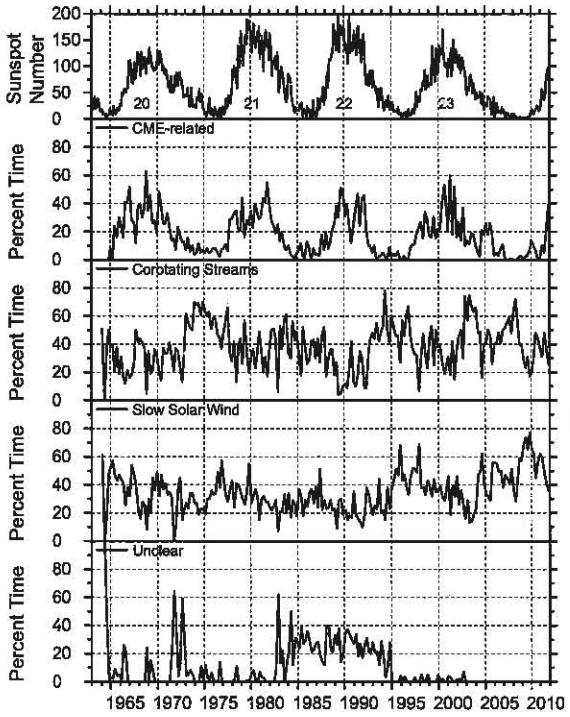

Fig. 4. Percentage of time when CME-associated flows, high-speed streams, slow solar wind, and unclear intervals were present during 3 solar rotation intervals in 1963–2011. The top panel shows the monthly sunspot number.

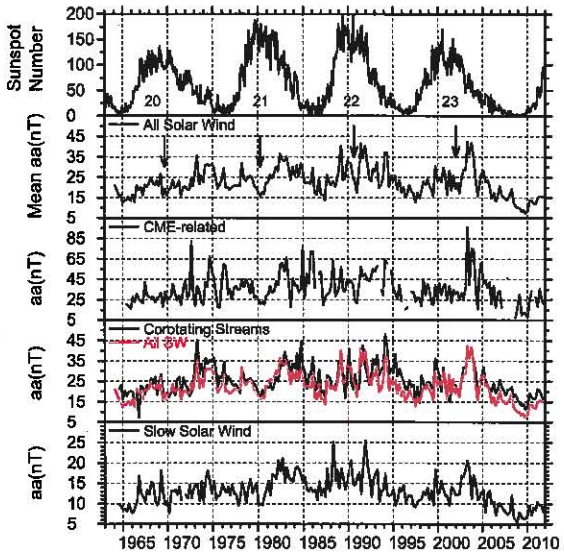

Fig. 5. The sunspot number (top panel) together with three-rotation averages of the *aa* geomagnetic index in all-solar-wind, and in CME-associated flows, corotating streams, and slow solar wind separately (note changes in vertical scale). Arrows indicate temporary depressions in *aa* around solar maximum related to the "Gnevyshev Gap". Note that the lowest values of *aa* during this period, in the solar minimum following cycle 23, are evident in all the solar wind flow types. The all-solar-wind results are overplotted on those for streams, showing that average values of *aa* tend to track those in streams, as previously noted by Richardson et al. (2001).

solar activity, note also the temporary decreases around solar maximum indicated by arrows, such that some of the lowest levels of geomagnetic activity actually occur close to solar maximum. These features (and others to be discussed below) may be related to the lack of energetic solar phenomena near solar maximum, termed the "Gnevyshev Gap" by Feminella & Storini 1997 who associate this with the temporary decrease in solar indices often found near sunspot maximum discussed by Gnevyshev (1967) and Gnevyshev (1977). (We note though that Kane 2005 has argued that the dip in *aa* in the Gnevyshev Gap does not strictly follow those in solar indices.) For a recent interpretation of the Gnevyshev Gap in terms of solar dynamo modeling, see Norton & Gallagher (2010).

Another notable feature in Figure 5 is the unusually low values of *aa* (at least since 1963), in the recent extended minimum following cycle 23 (see also Tsurutani et al. 2011). These low values are evident in the averages for each solar wind flow type suggesting that they are pervasive throughout the solar wind. The all-solar-wind *aa* graph is overplotted in red on the stream-associated graph, illustrating how average values of *aa* tend to track those associated with streams, as previously noted by Richardson et al. (2002). However, average values fall below those in streams in the recent minimum because of the prominent contribution of weak activity in slow solar wind, as illustrated in Figure 6 which shows the contribution of each flow type to the three-rotation *aa* averages, including the unusually high (~60%) contribution from slow solar wind in 2009 right at solar minimum. Figure 6 also shows the CME-associated flow contribution to *aa* that follows the solar activity cycle, and the stream-associated contribution that is most prominent during the declining phase/minimum. Another notable feature is that during the late declining phase of cycle 23, an increase in the contribution from CME-associated flows occurred in 2004–2006 together with a reduction in the stream-associated contribution that does not appear to have a counterpart in previous cycles.

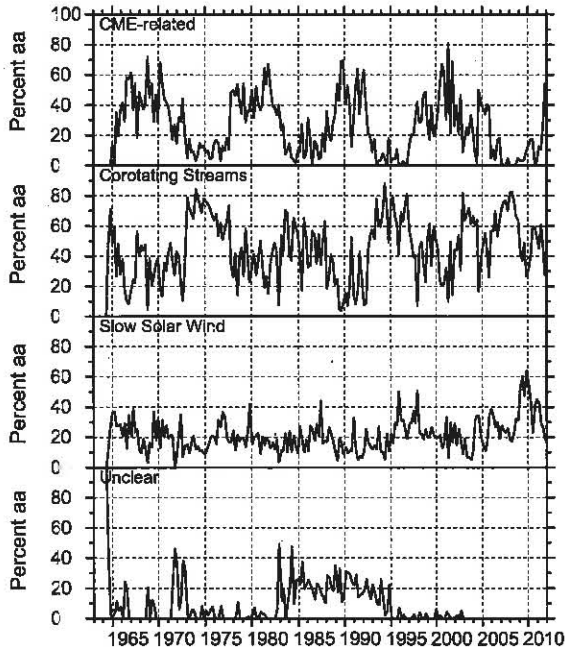

Fig. 6. Percentage of three-rotation averages of *aa* contributed by each solar wind flow type and by intervals of "unclear" flows.

Previous studies (e.g., Crooker et al. 1977; Crooker & Gringauz 1993) have suggested that $aa \sim V^2 B_s$, where B_s, the strength of the southward magnetic field component, is in turn limited by the magnetic field strength. Figure 7 examines variations in the solar and interplanetary magnetic field strengths and *aa* during cycles 20–24. The top panel shows Carrington-rotation averages of the mean solar magnetic field ("Sun as a star") measured by the Wilcox Solar Observatory since 1974. The mean solar field is dominated by the line-of-sight component of photospheric fields within ~0.5R_s of disk center, and daily measurements show positive and negative (outward and inward) oscillations that are well correlated with the direction of the IMF at Earth after allowing for the solar wind transit time to 1 AU (Scherrer et al. 1977). The root mean square of the daily measured fields is shown here. The second panel shows three-rotation averages of the *aa* geomagnetic index, while the bottom four panels show the interplanetary magnetic field intensity from 1964 to 2011, in all-solar-wind, CME-related solar wind, corotating high-speed streams, and slow solar wind; the all-solar-wind average is overplotted in red in the lower panels. Cycles 21–23 show variations in the solar and interplanetary magnetic fields and the *aa* index that tend to follow the sunspot cycle. Clear structures that appear in each data set illustrate the close association between solar and interplanetary magnetic fields, and geomagnetic activity. Note in particular the temporary

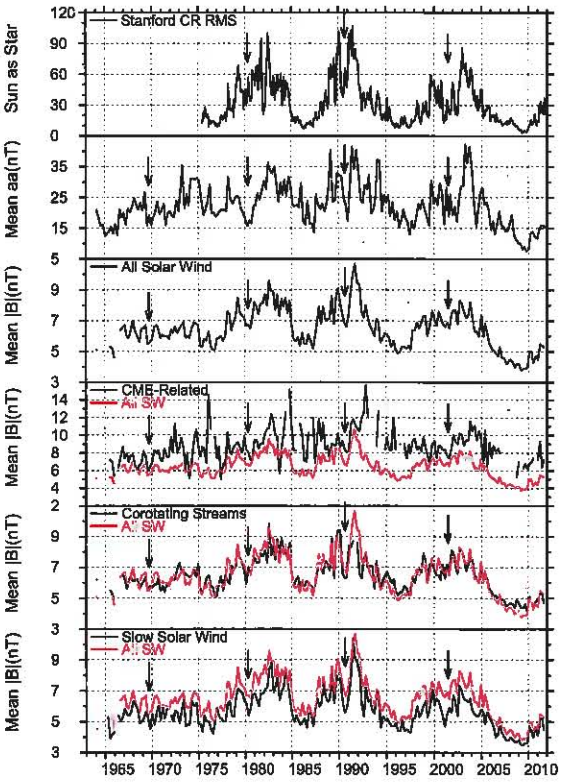

Fig. 7. Carrington-rotation (RMS) averages of the solar "Sun as a star" magnetic field observed by the Wilcox Solar Observatory together with three-rotation averages of the *aa* geomagnetic index, the interplanetary magnetic field strength in all-solar-wind flows (repeated in red in the lower three panels), and the field strength in CME-associated flows, corotating streams, and slow solar wind. Arrows indicate temporary depressions in all these parameters near solar maximum related to the "Gneveshev Gap".

decreases in solar and interplanetary fields and geomagnetic activity around solar maximum in these cycles, indicated by arrows, in the Gnevyshev Gaps. As has been previously noted (e.g., Hedgecock 1975), cycle 20 did not show a clear increase in the interplanetary magnetic field intensity (there are no Wilcox solar magnetic field observations for comparison), and the magnetic fields are relatively weak in all-solar-wind regions. The generally lower values of *aa* during cycle 20 than in later cycles are also consistent with a weaker IMF.

The unusually low values of geomagnetic activity (Tsurutani et al. 2011) and magnetic field strength (Smith & Balogh 2008; Connick et al. 2011) in the recent solar minimum are evident in Figure 7 and are observed in both slow solar wind and corotating streams. Field strengths within the few CME-associated flows observed in 2009–2010 are also weaker than those found during much of the period in Figure 7, indicating that the weaker fields during this minimum were manifested in both transient and quasi-stationary solar wind flows. Both the recent minimum and cycle 20 conform to the pattern previously discussed by Richardson et al. (2000, 2002) in that the mean all-solar-wind IMF field strength closely tracks the mean fields found in streams and slow solar wind. Our interpretation of this pattern, and of the remarkably similar variations in the solar and interplanetary magnetic fields, is that the variations in the average IMF intensity are closely related to solar magnetic field variations, and are predominantly manifested in the background, non-transient solar wind. In particular, we emphasize that average fields at 1 AU, even during higher solar activity levels, are not dominated by the contribution of magnetic fields in transients that pass the observing spacecraft – the solar cycle variation is essentially unchanged if the average field intensity is calculated using only the slow solar wind and stream intervals.

It has been suggested, however (Owens & Crooker, 2006), that the solar cycle increases in the IMF strength arise from closed field lines that are carried out by ICMEs to several AUs and are then opened by interchange reconnection. These field lines then add to the open magnetic flux in the heliosphere, and contribute to (and cannot be distinguished from) the background solar wind *outside* of the individual ICMEs that pass an observing spacecraft near the Earth. This model, using SOHO/LASCO CME rates (http://cdaw.gsfc.nasa.gov/CME_list/) as input and a characteristic time scale for reconnection of 50 days, can account for the observed variation in the IMF during solar cycle 23 fairly successfully. Unfortunately, there are no comparable CME observations to test the model for previous solar cycles, but we suggest that the occurrence of CME-associated flows might provide a reasonable proxy for the CME rate.

As noted above, the solar cycle variation in the IMF was much weaker in cycle 20 than in cycles 21–23. One possibility to account for this observation is that the CME rate was considerably lower in cycle 20 than in later cycles. However, the results in Figure 4 indicate that CMEs and associated flows were observed for similar fractions of time near the Earth during cycle 20 as in later cycles. This suggests that the CME rate was probably not substantially lower in cycle 20 but rather may have been comparable to that in later cycles.

To examine this further, Figure 8 shows one-rotation averages of the interplanetary magnetic field intensity for all-solar-wind plotted against the percentage of the time when CME-associated flows were present in each of the cycles 20–23. Assuming that the CME-associated flow occurrence is a reasonable proxy for the CME rate at the Sun (a caveat will be noted below), and the IMF strength is related to the magnetic flux added by ICMEs, we might then expect evidence of a

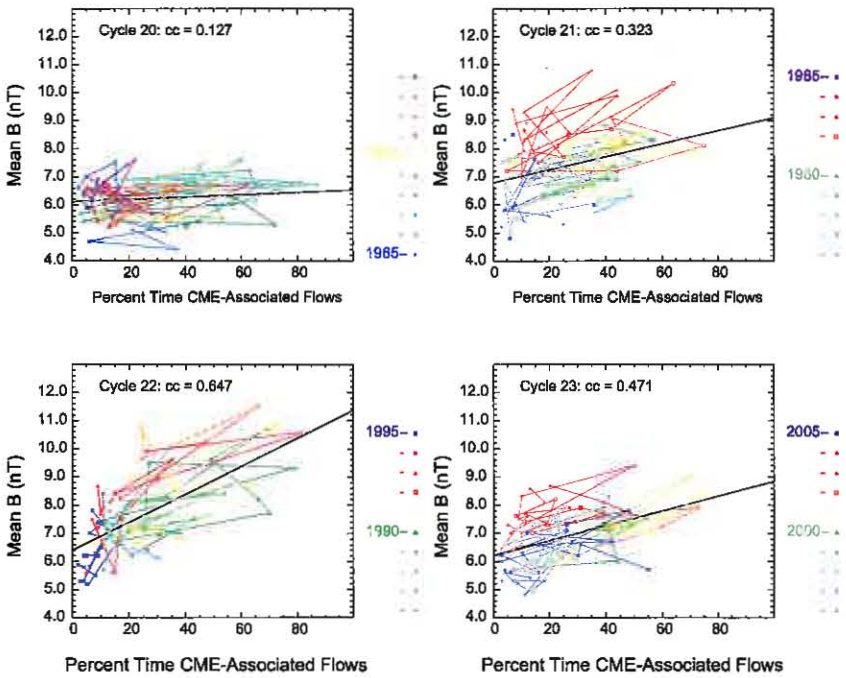

Fig. 8. The mean interplanetary magnetic field strength (one solar rotation averages) plotted against the percentage of time when CME-associated flows were present during cycles 20–23. The line/symbol color indicates the observation date. Cycles 21–23 show evidence of a positive correlation between field strength and ICME occurrence, possibly consistent with the proposal that magnetic flux carried out by ICMEs contributes to the solar cycle variation in field strength. However, no correlation is observed in cycle 20 where the near absence of a solar cycle field variation despite an increase in the occurrence of CME-associated flows would appear to present a challenge to this proposal.

positive correlation between the IMF strength and the CME-associated flow occurrence in each cycle, similar to that found between IMF intensity and LASCO CME rate in cycle 23 by Owens et al. (2008) (cf. their Fig. 1). The color of the line/symbol in each panel in Figure 8 indicates the time of observation. While there is a general increase in IMF intensity for increasing CME-associated flow occurrence in cycles 21–23 which may support the Owens & Crooker (2006) model, the distribution of points for cycle 20 is relatively flat because there was little increase in the IMF strength, despite the increase in the occurrence of CME-associated flows, as solar activity levels increased. This observation would appear to pose a challenge to the Owens & Crooker (2006) model.

One possibility is that the ICMEs in cycle 20 carried substantially less magnetic flux than in later cycles. The mean field in CME-associated flows (which include sheath regions as well as ICMEs) was indeed weaker (7.9 nT) during the maximum of cycle 20 compared with 9.1 nT in cycle 21, 10.1 nT in cycle 22, and 8.8 nT in cycle 23, but the difference seems too small to account for the near absence of a solar cycle field variation in cycle 20. The ICMEs might have had smaller volumes on average, and hence carried less magnetic flux, but presumably this would also have reduced the amount of time when CME-associated flows were present, which was not observed. A smaller reconnection time constant would contribute to a smaller magnetic cycle (Owens & Crooker 2006), though it is not clear why this should be a feature only of cycle 20.

A caveat to the results in Figure 8 is that it has been noted that the ICME rate at the Earth during cycle 23 did not track the CME rate at the Sun accurately (Riley et al. 2006), so likewise, the occurrence of CME-associated flows during cycle 20 may also not fully reflect variations in the CME rate. On the other hand, when the CME and ICME rates diverged in cycle 23, the CME rate actually rose more rapidly than the ICME rate. Hence, it is possible that the CME rate in cycle 20 similarly may have increased even more rapidly than is indicated by the CME-associated flow occurrence at 1 AU, in which case the absence of the solar cycle variation in the IMF intensity is even more puzzling. Thus, in summary, we suggest that the observed increase in the occurrence of near-Earth CME-associated flows during cycle 20, indicative of an increase in the CME rate at the Sun, together with the weak increase in the interplanetary magnetic field strength during this cycle, may pose a challenge to Owens & Crooker (2006) proposal that solar cycle variations in the strength of the interplanetary magnetic field are associated with magnetic flux carried out by ICMEs.

Figure 9 examines average solar wind speeds in 1963–2011. We again show the monthly sunspot number and three-rotation averaged *aa* index, together with three-rotation averages of the solar wind speed for all-solar-wind and separately for corotating streams and CME-associated flows. The solar wind speed clearly shows little correlation with solar activity levels. In fact, there is a tendency for local minima in the solar wind speed, including in CME-associated flows, in the Gnevyshev Gaps (indicated by arrows) near solar maximum. Thus, some of the slowest solar winds during the solar cycle can occur close to solar maximum. The highest speeds tend to occur during the declining phase of the cycle when corotating streams are predominant, but the persistence of these flows varies from cycle to cycle. In particular, in cycle 23, average flow speeds exceeding 500 km s^{-1} associated with corotating streams were predominant only in 2003 but were present for ~4 years in the decline of cycle 20. Average solar wind speeds in the recent solar minimum were also evidently the lowest observed since

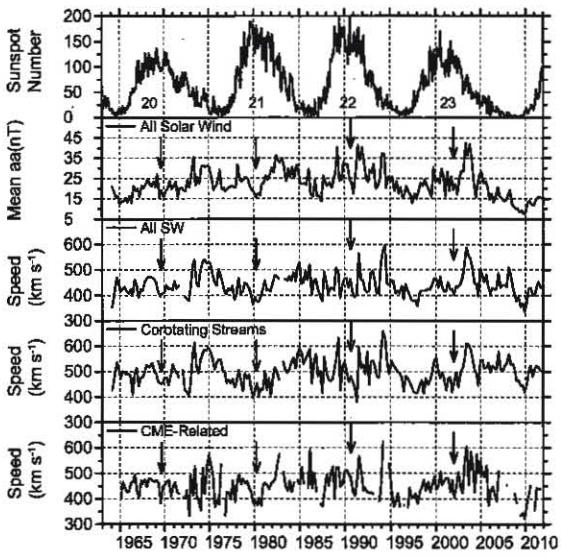

Fig. 9. Three-rotation averages of the solar wind speed in all-solar-wind and in corotating streams and CME-associated flows during 1963–2011 are shown in the bottom three panels. The top panels show the monthly sunspot number and three-rotation averages of the *aa* geomagnetic index. Arrows indicate local minima in the solar wind speed and geomagnetic activity near solar maximum.

the very earliest in-situ observations. As also suggested by Tsurutani et al. (2011), the above results indicate that the low geomagnetic activity levels in the recent minimum were a combination of low solar wind speeds (Fig. 9) due to the prevalence of slow solar wind at the expense of streams (Figs. 4 and 6), and weak interplanetary magnetic fields that are related to weak solar magnetic fields (Fig. 7). We also note that the CME-related flows in cycle 23 were slower (averages are below ~500 km s^{-1}) during the ascending phase of the cycle than during the descending phase, where average speeds were typically ~500–600 km s^{-1}. This asymmetry may reflect the faster ambient solar wind speeds evident in Figure 9, and the increased frequency of fast (>1000 km s^{-1}) ICME-driven interplanetary shocks noted by Cane et al. (2006), during the declining phase of this cycle.

Figure 10 shows three-rotation averages of *aa* plotted against average values of V^2B_s for all-solar-wind, CME-associated flows (note the different scale), high-speed streams, and slow solar wind, in 1964–2011. The positive correlations again indicate that variations in V^2B_s are the dominant factor determining the geoeffectiveness of the different types of solar wind flows. As previously noted by Richardson et al. (2002) using a subset of these data, the fits through the data are similar in each case, though with the extended data set, CME-associated flows, while extending to higher *aa* values than other flow types also have a slightly weaker dependence on V^2B_s. The generally lower activity levels associated with slow solar wind are also evident.

4. Summary

- We have classified near-Earth solar wind structures since the beginning of in-situ observations in 1963–2011, encompassing solar cycles 20–23 and the ascending phase of cycle 24, into CME-associated flows (including ICMEs

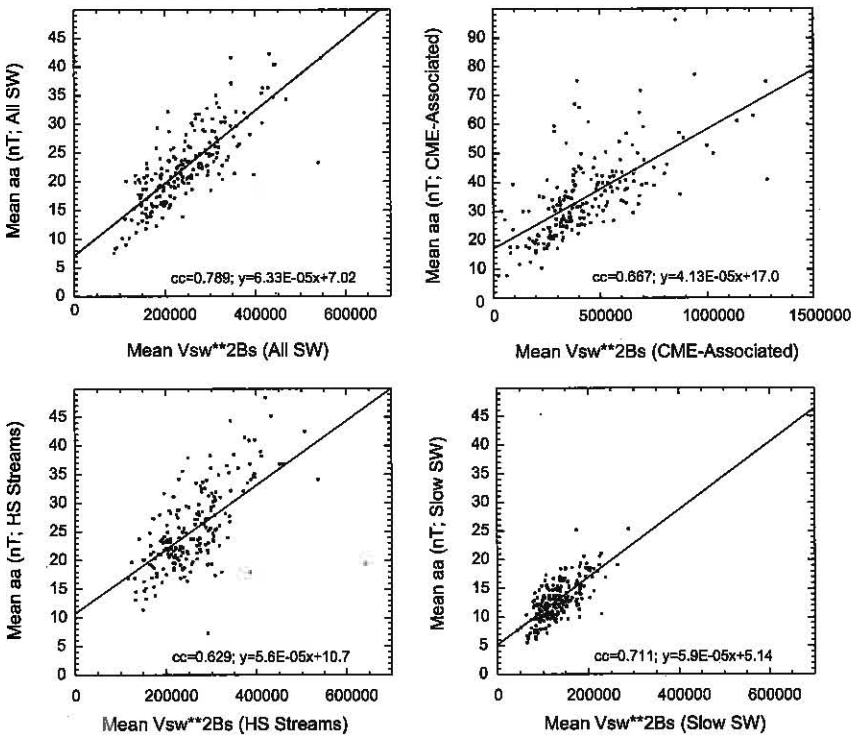

Fig. 10. Three-rotation means of *aa* plotted vs. V^2B_s (in units of (km s^{-1})^2 nT) for all-solar-wind, CME-associated flows, high-speed streams, and slow solar wind, in 1964–2011.

and post-shock/sheath regions), corotating streams and slow solar wind, using the OMNI data and additional data sets, extending earlier studies of this type that commenced with observations in 1972 (Richardson et al. 2000, 2001, 2002; Richardson 2006).

- The solar ("Sun as a star") and interplanetary magnetic field strengths in cycles 21–23 show variations that are similar in each data set, including temporary reductions close to solar maximum. Geomagnetic activity also shows similar reductions near solar maximum, and variations that are similar to those observed in the IMF and solar wind speed.
- The low levels of geomagnetic activity during the recent solar minimum following cycle 23 are related to low solar wind speeds, due to a prevalence of slow solar wind rather than streams and unusually weak interplanetary fields that are found in all-solar-wind flows and reflect weak solar magnetic fields.
- The declining phase of cycle 23 is also characterized by an unusual persistence of CME-associated geomagnetic activity, extending to 2006, and a ~1-year period in 2003 in which enhanced activity associated with streams was dominant, including some of the highest (three-rotation averaged) levels found during the study period.
- Analysis of the weak solar cycle 20 suggests that CME-associated flows were present for a similar fraction of the time (~40%) as found in cycles 21–23, suggesting that the CME rate during this cycle was also comparable. The relatively weak increase in the interplanetary magnetic field intensity during cycle 20 may pose a problem for models of the solar cycle IMF variation that assume that field lines transported by ICMEs contribute to solar cycle variations in the IMF strength.

Acknowledgements. We thank the many researchers who have made available near-Earth magnetic field, plasma and energetic particle data that have contributed to the solar wind identifications, and to J. King and colleagues at the Space Physics Data Facility at GSFC for compiling the OMNI database. The Thule neutron monitor (P.I. John Bieber) is supported by the University of Delaware and the Bartol Research Institute. Data were obtained from the Bartol web site (http://neutronm.bartol.udel.edu/). We acknowledge discussions with E.W. Cliver that prompted extending the solar wind classification back through cycle 20.

References

Barnden, L.R., Forbush decreases 1966–1972; Their solar and interplanetary associations and their anisotropies, *Proc. 13th Int. Cosmic Ray Conf.*, **2**, 1271, 1973a.

Barnden, L.R., Forbush decreases 1966–1972; The large-scale magnetic field configuration associated with Forbush decreases, *Proc. 13th Int. Cosmic Ray Conf.*, **2**, 1277, 1973b.

Belcher, J.W., and L. Davis, Large amplitude Alfvén waves in the interplanetary medium, 2, *J. Geophys. Res.*, **76**, 3534, 1971.

Burlaga, L.F., and R.P. Lepping, The causes of recurrent geomagnetic storms, *Planet. Space Sci.*, **25**, 1151, 1977.

Burlaga, L.F., E. Sittler, F. Mariani, and R. Schwenn, Magnetic loop behind an interplanetary shock: Voyager, Helios and IMP 8 observations, *J. Geophys. Res.*, **86**, 6673, 1981.

Cane, H.V., Cosmic ray decreases and magnetic clouds, *J. Geophys. Res*, **98**, 3509, 1993.

Cane, H.V., Coronal mass ejections and Forbush decreases, *Space Sci. Rev.*, **93**, 55, 2000.

Cane, H.V., and D. Lario, An introduction to CMEs and energetic particles, *Space Sci. Rev.*, **123**, 45, 2006.

Cane, H.V., and I.G. Richardson, Interplanetary coronal mass ejections in the near-Earth solar wind during 1996–2002, *J. Geophys. Res.*, **108**, 1156, DOI: 10.1029/2002JA009817, 2003.

Cane, H.V., I.G. Richardson, and T.T. von Rosenvinge, Cosmic ray decreases and particle acceleration in 1978–1982 and the associated solar wind structures, *J. Geophys. Res.*, **98**, 13295, 1993.

Cane, H.V., I.G. Richardson, and T.T. von Rosenvinge, Cosmic ray decreases: 1964–1994, *J. Geophys. Res.*, **101**, 21561, 1996.

Cane, H.V., R.A. Mewaldt, C.M.S. Cohen, and T.T. von Rosenvinge, Role of flares and shocks in determining solar energetic particle abundances, *J. Geophys. Res.*, **111**, A06S90, DOI: 10.1029/2002JA009817, 2006.

Chao, J.K., and R.P. Lepping, A Correlative study of SSC's, interplanetary shocks, and solar activity, *J. Geophys. Res.*, **79**, 1799, 1974.

Connick, D.E., C.W. Smith, and N.A. Schwadron, Interplanetary magnetic flux depletion during protracted solar minima, *Astrophys. J.*, **727**, 8, DOI: 10.1088/0004-637X/727/1/8, 2011.

Crooker, N.U., and K.I. Gringauz, On the low correlations between long-term averages of solar wind speed and geomagnetic activity after 1976, *J. Geophys. Res.*, **98**, 59, 1993.

Crooker, N.U., J. Feynman, and J.T. Gosling, On the high correlation between long-term averages of solar wind speed and geomagnetic activity, *J. Geophys. Res.*, **82**, 1933, 1977.

Dungey, J.W., Interplanetary magnetic field and the auroral zones, *Phys. Rev. Lett.*, **6**, 47, 1961.

Echer, E., W.D. Gonzalez, B.T. Tsurutani, and A.L.C. Gonzalez, Interplanetary conditions causing intense geomagnetic storms ($Dst \leq -100$ nT) during solar cycle 23 (1996–2006), *J. Geophys. Res.*, **113**, A05221, 2008.

Emery, B.A., I.G. Richardson, D.S. Evans, and F.J. Rich, Solar wind structure sources and periodicities of auroral electron power over three solar cycles, *J. Atmosph. Solar-Terr. Phys.*, **71**, 1157, DOI: 10.1016/j.jastp.2008.08.005, 2009.

Emery, B.A., I.G. Richardson, D.S. Evans, F.J. Rich, and G.R. Wilson, Solar rotational periodicities and the semiannual variation in the solar wind, radiation belt, and aurora, *Solar Phys.*, **274**, 399, DOI: 10.1007/s11207-011-9758-x, 2011.

Feminella, F., and M. Storini, Large scale dynamical phenomena during solar activity cycles, *A&A*, **322**, 311, 1997.

Feldman, W.C., J.R. Asbridge, S.J. Bame, E.E. Fenimore, and J.T. Gosling, Origin of solar wind interstream flows: Near Equitorial coronal streamers, *J. Geophys. Res.*, **86**, 5408, 1981.

Forbush, S.E., On the effects in the cosmic ray intensity observed during the recent magnetic storm, *Phys. Rev.*, **51**, 1108, 1937.

Gnevyshev, M.N., On the 11-years cycle of solar activity, *Sol. Phys.*, **1**, 107, 1967.

Gnevyshev, M.N., Essential features of the 11 year solar cycle, *Sol. Phys.*, **51**, 175, 1977.

Gold, T., Discussion of shock waves and rarefied gases, in *Gas Dynamics of Cosmic Clouds*, North-Holland Publishing Co, Amsterdam, 193, 1955.

Gosling, J.T., J.R. Asbridge, S.J. Bame, A.H. Hundhausen, and I.B. Strong, Discontinuities in the solar wind associated with sudden geomagnetic impulses and sudden commencements, *J. Geophys. Res.*, **72**, 3357, 1967.

Gosling, J.T., D.J McComas, J.L. Phillips, and S.J. Bame, Geomagnetic activity associated with Earth passage of interplanetary shock disturbances and coronal mass ejections, **96**, 7831, 1991.

Hedgecock, P.C., Measurements of the interplanetary magnetic field in relation to the modulation of cosmic rays, *Solar Phys.*, **42**, 497, 1975.

Huttunen, K., and H. Koskinen, Importance of post-shock streams and sheath region as drivers of intense magnetospheric storms and high-latitude activity, *Ann. Geophys.*, **22**, 1729, 2004.

Iucci, N., M. Parisi, M. Storini, and G. Villoresi, High speed solar wind streams and galactic cosmic ray modulation, *Nuovo Cimento*, **2C**, 421, 1979.

Ji, E.-Y., Y.-J. Moon, and K.-H. Kim, Statistical comparison of interplanetary conditions causing intense geomagnetic storms ($Dst \leq -100$ nT), *J. Geophys. Res.*, **115**, A10232, DOI: 10.1029/2009JA015112, 2010.

Kane, R.P., Which one is the "Gnevyshev" gap? *Solar Phys.*, **229**, 387, 2005.

King, J.H., and N.E. Papitashvili, Solar wind spatial scales in and comparisons of hourly wind and ACE plasma and field data, *J. Geophys. Res.*, **110**, 2104, 2005.

Klecker, B., H. Kunow, H.V. Cane, S. Dalla, B. Heber, et al., Energetic particle observations, *Space Sci. Rev.*, **123**, 217, 2006.

Klein, L.W., and L.F. Burlaga, Interplanetary magnetic clouds at 1 AU, *J. Geophys. Res.*, **87**, 613, 1982.

Krieger, A.S., A.F. Timothy, and E.C. Roelof, A coronal hole and its identification as the source of a high velocity solar wind stream, *Sol. Phys.*, **29**, 505, 1973.

Love, J.J., Long-term biases in geomagnetic *K* and *aa* indices, *Ann. Geophys*, **29**, 1365, 2011.

Mayaud, P.N., The *aa* indices: A 100-year series characterising the geomagnetic activity, *J. Geophys. Res.*, **77**, 6870, 1972.

Menvielle, M., and A. Berthelier, The K-derived planetary indices: Description and availability, *Rev. Geophys.*, **29**, 415, DOI: 10.1029/91RG00994, 1991.

Norton, A.A., and J.C. Gallagher, Solar-cycle characteristics examined in separate hemispheres: Phase, Gnevyshev gap, and length of minimum, *Solar Phys.*, **261**, 193, 2010.

O'Brien, T.P., and R.L. McPherron, An empirical phase space analysis of ring current dynamics: Solar wind control of injection and decay, *J. Geophys. Res.*, **105**, 7707, 2000.

Owens, M.J., and N.U. Crooker, Coronal mass ejections and magnetic flux buildup in the heliosphere, *J. Geophys. Res.*, **111**, A10104, DOI: 10.1029/2006JA011641, 2006.

Owens, M.J., N.U. Crooker, N.A. Schwadron, T.S. Horbury, S. Yashiro, et al., Conservation of open solar magnetic flux and the floor in the heliospheric magnetic field, *Geophys. Res. Lett.*, **35**, L20108, DOI: 10.1029/2008GL035813, 2008.

Richardson, I.G., Energetic particles and corotating interaction regions in the solar wind, *Space Sci. Rev.*, **111**, 267, 2004.

Richardson, I.G., The formation of CIRs at stream-stream interfaces and resultant geomagnetic activity. in *Recurrent Magnetic Storms: Corotating Solar Wind Streams*, ed. B.T., Tsurutani et al., A.G.U. Geophysical Monograph, **167**, 45, 2006.

Richardson, I.G., and H.V. Cane, Signatures of shock drivers in the solar wind and their dependence on the solar source location, *J. Geophys. Res.*, **98**, 15295, 1993.

Richardson, I.G., and H.V. Cane, Regions of abnormally low proton temperature in the solar wind (1965–1991) and their association with ejecta, *J. Geophys. Res.*, **100**, 23397, 1995.

Richardson, I.G., and H.V. Cane, Near-Earth interplanetary coronal mass ejections during solar cycle 23 (1996–2009): Catalog and summary of properties, *Solar Phys.*, **264**, 189, 2010.

Richardson, I.G., and H.V. Cane, Geoeffectiveness (*Dst* and *Kp*) of interplanetary coronal mass ejections during 1995–2009 and implications for storm forecasting, *Space Weather*, **9**, S07005, DOI: 10.1029/2011SW000670, 2011a.

Richardson, I.G., and H.V. Cane, Galactic Cosmic Ray Intensity Response to Interplanetary Coronal Mass Ejections/Magnetic Clouds in 1995–2009, *Solar Phys*, **270**, 609, DOI: 10.1007/s11207-011-9774-x, 2011b.

Richardson, I.G., G. Wibberenz, and H.V. Cane, The relationship between recurring cosmic ray depressions and corotating solar wind streams at $\leq$1 AU: IMP 8 and Helios 1 and 2 anticoincidence guard rate observations, *J. Geophys. Res.*, **101**, 13483, 1996.

Richardson, I.G., C.J. Farrugia, and H.V. Cane, A statistical study of the behavior of the electron temperature in ejecta, *J. Geophys. Res.*, **102**, 4691, 1997.

Richardson, I.G., H.V. Cane, and G. Wibberenz, A 22-year dependence in the size of near-ecliptic corotating cosmic ray depressions during five solar minima, *J. Geophys. Res.*, **104**, 12549, 1999.

Richardson, I.G., E.W. Cliver, and H.V. Cane, Sources of geomagnetic activity over the solar cycle: Relative importance of CMEs, high-speed streams, and slow solar wind, *J. Geophys. Res.*, **105**, 18203, 2000.

Richardson, I.G., E.W. Cliver, and H.V. Cane, Sources of geomagnetic storms for solar minimum and maximum conditions during 1972–2000, *Geophys. Res. Lett.*, **28**, 2569, 2001.

Richardson, I.G., H.V. Cane, and E.W. Cliver, Sources of geomagnetic activity during nearly three solar cycles (1972–2000), *J. Geophys. Res.*, **107**, DOI: 10.1029/2001JA000504, 2002.

Richardson, I.G., D.F. Webb, J. Zhang, D.B. Berdichevsky, D.A. Biesecker, et al., Major geomagnetic storms ($Dst \leq -100$ nT) generated by corotating interaction regions, *J. Geophys. Res.*, **111**, A07S09, DOI: 10.1029/2005JA011476, 2006.

Riley, P., C. Schatzman, H.V. Cane, I.G. Richardson, and N. Gopalswamy, On the rates of coronal mass ejections: Remote solar and in situ observations, *Astrophys. J.*, **647**, 648, 2006.

Robbrecht, E., D. Berghmans, and R.A.M. Van der Linden, Automated LASCO CME catalog for solar cycle 23: Are CMEs scale invariant? *Astrophys. J*, **691**, 1222, DOI: 10.1088/0004-637X/691/2/1222, 2009.

Russell, C.T., J.G. Luhmann, and L.K. Jian, How unprecedented a solar minimum? *Rev. Geophys.*, **48**, RG2004, DOI: 10.1029/2009RG000316, 2010.

Sanderson, T.R., J. Beeck, R.G. Marsden, C. Tranquille, K.-P. Wenzel, R.B. McKibben, and E.J. Smith, A study of the relation between magnetic clouds and Forbush decreases, *Proc. 21st Int. Cosmic Ray Conf.*, **6**, 251, 1990.

Scherrer, P.H., J.M. Wilcox, L. Svalgaard, T.L. Duvall Jr., P.H. Dittmer, and E.K. Gustafson, The mean magnetic field of the Sun: Observations at Stanford, *Solar Phys.*, **54**, 353, 1977.

Sheeley Jr., N.R., J.W. Harvey, and W.C. Feldman, Coronal holes, solar wind streams, and recurrent geomagnetic disturbances, 1973–1976, *Solar Phys.*, **49**, 271, 1976.

Sheeley Jr., N.R., J.S. Asbridge, S.J. Bame, and J.W. Harvey, A pictorial comparison of interplanetary magnetic field polarity, solar wind speed, and geomagnetic disturbance index during the sunspot cycle, *Solar Phys.*, **52**, 485, 1977.

Simpson, J.A., A brief history of recurrent solar modulation of the galactic cosmic-rays, *Space Sci. Rev.*, **83**, 169, 1998.

Simpson, J.A., H.W. Babcock, and H.D. Babcock, Association of a "unipolar" magnetic region on the Sun with changes of primary cosmic-ray intensity, *Phys. Rev.*, **98**, 1402, 1955.

Smith, E.J., and A. Balogh, Decrease in heliospheric magnetic flux in this solar minimum: Recent Ulysses magnetic field observations, *Geophys. Res. Lett.*, **35**, L22103, DOI: 10.1029/2008GL035345, 2008.

Sugiura, M., Hourly values of equatorial *Dst* for the IGY, *Ann. Int. Geophys. Year*, **35**, 9, 1964.

Tsurutani, B.T., and W.D. Gonzalez, The cause of high intensity long-duration continuous AE activity (HILDCAAs); Interplanetary Alfvén wave trains, *Planet. Space Sci.*, **35**, 405, 1987.

Tsurutani, B.T., E.J. Smith, W.D. Gonzalez, and F. Tang, Origin of interplanetary southward magnetic fields responsible for major magnetic storms near solar maximum (1978–1979), **93**, 8519, 1988.

Tsurutani, B.T., and W.D. Gonzalez, The interplanetary causes of magnetic storms: A review, in *Magnetic Storms*, ed. B.T., Tsurutani, W.D. Gonzalez, Y. Kamide, and J.K. Arballo, A.G.U. Geophys. Monogr. Ser., Vol. **98**, AGU, Washington, DC, 77, 1997.

Tsurutani, B.T., R.L. McPherron, W.D. Gonzalez, G. Lu, N. Gopalswamy, and F.L. Guarnieri, Magnetic storms caused by corotating solar wind streams, in *Recurrent Magnetic Storms: Corotating Solar Wind Streams*, ed. B.T., Tsurutani, R.L. McPherron, W.D. Gonzalez, G. Lu, J.H.A. Sobral, and N. Gopalswamy, A.G.U. Geophysical Monograph, **167**, 1, 2006.

Tsurutani, B.T., E. Echer, and W.D. Gonzalez, The solar and interplanetary causes of the recent minimum in geomagnetic activity (MGA23): a combination of midlatitude small coronal holes, low IMF BZ variances, low solar wind speeds and low solar magnetic fields, *Ann. Geophys.*, **29**, 839, DOI: 10.5194/angeo-29-839-2011, 2011.

Turner, N.E., W.D. Cramer, S.K. Earles, and B.A. Emery, Geoefficiency and energy partitioning in CIR-driven and CME-driven storms, *J. Atmosph. Solar-Terr. Phys.*, **71**, 1023, 2009.

Van Hollebeke, M.A., J.R. Wang, and F.B. McDonald, *A catalogue of solar cosmic ray events IMPs IV and V (May 1967–Dec. 1972)*, NASA Goddard Space Flight Center, X-661-74-27, 1974.

Wang, C., C.X. Li, Z.H. Huang, and J.D. Richardson, Effect of interplanetary shock strengths and orientations on storm sudden commencement rise times, *Geophys. Res. Lett.*, **33**, L14104, DOI: 10.1029/2006GL025966, 2006.

Webb, D.F., and R.A. Howard, The solar cycle variation of coronal mass ejections and the solar wind mass flux, *J. Geophys. Res.*, **99**, 4201, 1994.

Wilson, R.M., Geomagnetic response to magnetic clouds, *Planet. Space Sci.*, **35**, 329, 1987.

Wilson, R.M., On the behavior of the *Dst* geomagnetic index in the vicinity of magnetic cloud passage at Earth, *J. Geophys. Res.*, **95**, 215, 1988.

Yashiro, S., N. Gopalswamy, G. Michalek, O.C. St. Cyr, S.-P. Plunkett, N.B. Rich, and R.A. Howard, A catalog of white light coronal mass ejections observed by the SOHO spacecraft, *J. Geophys. Res.*, **109**, A07105, 2004.

Zhang, J., I.G. Richardson, D.F. Webb, N. Gopalswamy, E. Huttunen, et al., Solar and interplanetary sources of major geomagnetic storms ($Dst \leq -100$ nT) during 1996–2005, *J. Geophys. Res.*, **112**, A12105, DOI: 10.1029/2007JA012332, 2007.

Zhao, L., T.H. Zurbuchen, and L.A. Fisk, Global distribution of the solar wind during solar cycle 23: ACE observations, *Geophys. Res. Lett.*, **36**, 14104, DOI: 10.1029/2009GL039181, 2009.

Zirker, J.B., (ed.), *Coronal Holes and High Speed Wind Streams*, Skylab Solar Workshop, Colorado University Press, Boulder, CO, 1977.

Zurbuchen, T.H., and I.G. Richardson, In-situ solar wind and magnetic field signatures of interplanetary coronal mass ejections, *Space Sci. Rev.*, **123**, 31–34, 2006.